Nonequilibrium Viscous Shock-Layer Flows over Blunt Sphere-Cones at Angle of Attack

S. Swaminathan,* M.D. Kim,* and Clark H. Lewis†
Virginia Polytechnic Institute and State University, Blacksburg, Virginia

A computer program for predicting the three-dimensional nonequilibrium viscous shock-layer flows over blunt sphere-cones at angle of attack has been developed. The method used is the viscous shock-layer approach for nonequilibrium, multicomponent ionizing air. Analysis of flowfields over a sphere-cone has been performed for both shock-slip and no-shock-slip conditions and the results are compared. This code is capable of analyzing equilibrium and noncatalytic wall boundary conditions, whereas the diffusion model is limited to binary diffusion. Results from this code have been compared with those from another code for the axisymmetric case, while the three-dimensional results are presented around the entire body at 10 deg angle of attack.

Nomenclature

A_0-A_5 = coefficients of the parabolic partial differential equations
CFS, CFW = skin-friction coefficient in the streamwise and transverse directions
C_i = concentration of species i
C_p = specific heat at constant pressure
$\hat{C}_{pi}$ = species specific heat
D_i = binary diffusion coefficient
E-/cc = electron concentration per cubic centimeter
ECW = equilibrium catalytic wall
FCW = fully catalytic wall
h = static enthalpy, $h/^*u_\infty^2$
H = stagnation enthalpy, H^*/U_∞^2
$\hat{H}_i$ = species specific enthalpy
h_1, h_2, h_3 = shape factors for a general orthogonal coordinate system
J_i = diffusion mass flow term
k = thermal conductivity
k_{br} = backward rate constant
k_{fr} = forward rate constant
Le = Lewis number
M = molecular weight
$\bar{M}$ = mixture molecular weight
M_∞ = freestream Mach number
NCW = noncatalytic wall
NJ = number of species plus catalytic third bodies, $NS+NZ$
NR = number of chemical reactions
NS = number of species
NSH = shock standoff distance, n_{sh}
$NSHP$ = $\partial n_{sh}/\partial\xi$
NSS = no shock slip
NZ = number of catalytic third bodies
p = pressure, $p^*/\rho_\infty U_\infty^2$
PG = perfect gas
PHI = circumferential coordinate
$PINF$ = freestream pressure
Pr = Prandtl number
PW = wall pressure
q_w = heat-transfer rate at the wall
R = gas constant, ft^2/s^2R
Re = Reynolds number, $Re=\rho_\infty U_\infty R_n^*/\mu_\infty$
R_n^* = nose radius, ft
SORN = s^*/R_n^*
SS = shock slip
$STINF$ = Stanton number, $q_w^*/\rho_\infty U_\infty (H_0^*-H_w^*)$
s, n, ϕ = nondimensional surface-oriented coordinate system
T = temperature, $T^*/T_{ref}=T^*/(\gamma-1)T_\infty M_\infty^2$
U_∞ = freestream velocity, ft/s
u, v, w = velocity components, $u^*/U_\infty, v^*/U_\infty, w^*/U_\infty$
W = dependent variable
$\dot{w}_i$ = species production term
Y = distance normal to body
α = angle of attack, deg
ϵ = Reynolds number parameters, $\epsilon^2=\mu_{ref}^*/\rho_\infty u_\infty R_n^*$
μ = viscosity, μ^*/μ_{ref}
μ_{ref} = reference viscosity, $\mu^*(T_{ref})$
ξ, η, ζ = normalized surface-oriented coordinates
ρ = density, ρ^*/ρ_∞^*
σ = shock angle
α_{ri} = stoichiometric coefficients for reactants
β_{ri} = stoichiometric coefficients for products

Superscripts

$\bar{(\ )}$ = normalized variable
$(\ )^*$ = dimensional variable
$\tilde{(\ )}$ = shock-normal coordinate system
$\hat{(\ )}$ = interpolated data

Subscripts

eq = equilibrium value
i = species i
ref = dimensional reference conditions
sh = conditions behind the bow-shock
w = wall conditions
ζ = derivative with respect to ζ
∞ = dimensional freestream conditions
0 = stagnation conditions

Received June 24, 1982; revision received Jan. 10, 1983.

*Graduate Student, Aerospace and Ocean Engineering Department. Student Member AIAA.

†Professor, Aerospace and Ocean Engineering Department. Associate Fellow AIAA.

Introduction

THE viscous shock-layer equations, because of their advantages and accurate predictions with reasonable cost, are widely used as a tool for engineering calculations. These equations treat the entire flowfield from body to bow-shock in a uniform manner; hence the displacement effects and the outer boundary conditions can be accurately modeled. The governing partial differential equations are parabolic in

both streamwise and crossflow directions, thus making solutions far downstream of long re-entry vehicles possible with reasonable expense. The low densities encountered at high altitudes cause low Reynolds numbers, which make the classical inviscid/boundary-layer approach difficult to use. These advantages of viscous shock-layer equations inspired many investigators to apply viscous shock-layer equations for more complicated problems.

Davis[1] solved the shock-layer equations for laminar perfect gas flows over analytic bodies and Srivastava et al.[2] treated the problem of curvature discontinuity on a sphere-cone. Miner and Lewis[3,4] treated a seven species air mixture consisting of N, O, N_2, O_2, NO, NO^+, and e^- with finite-rate chemical reactions over nonanalytic blunt bodies such as sphere-cones at zero lift. Three-dimensional perfect gas flowfields with wall slip were analyzed by Murray and Lewis.[5,6] Szema and Lewis[7] extended the three-dimensional viscous shock-layer method to include laminar, transitional, and/or turbulent shock-layer flows. Thareja et al.[8] studied the effects of chemical equilibrium on three-dimensional viscous shock-layer analysis of hypersonic laminar or turbulent flows.

The main purpose of this paper is to study nonequilibrium three-dimensional flowfields over sphere-cones at angle of attack. This study was conducted in order to develop a code to predict, to a fair accuracy, the surface-measurable quantities over a sphere-cone and to provide initial-data plane profiles for a code to analyze the nonequilibrium flow over the windward side of the Space Shuttle, within reasonable computing time. The temperatures involved in re-entry flowfields are very high, causing dissociation and ionization of atmospheric molecules. Ionization affects transport phenomena and, at higher entry speeds, radiative transfer and communications. Since the re-entry speeds of the Space Shuttle are not high enough to cause communication blackout, the concentration of the electrons in the shock layer was considered to be of secondary importance; hence, some simplifications were assumed. Seven species ionizing air is considered as the medium, and it is assumed that chemical reactions proceed at finite rate. Since the behavior of electrons in the shock layer was of secondary importance, the effect of vibrational temperature was not included in the present study.

It has been observed from previous studies that the assumption of binary diffusion with constant Lewis-Semenov numbers gives a reasonably accurate solution of surface-measurable quantities. In addition, Blottner's study[9] of nonequilibrium, laminar boundary-layer flow of ionized air showed that the electron density was slightly changed with the simpler diffusion model. The inclusion of multicomponent diffusion would increase the computing time considerably; hence, multicomponent diffusion and the effects of ambipolar diffusion were not included in this study. For the same reasons, the effect of conduction of heat in the electron gas is not accounted for in the present study.

In order to validate the results from this code, one has to compare the results from this code to those from earlier codes or experimental results. Due to the wealth of experimental results, RAMC, a 9-deg half-angle sphere-cone is used as a test case. Analysis is performed at two different freestream conditions; first at 83.82 km (275 kft) with an inverse Reynolds number parameter and an ϵ of 0.3107, and second at 70.104 km (230 kft) with an ϵ of 0.1052. The freestream

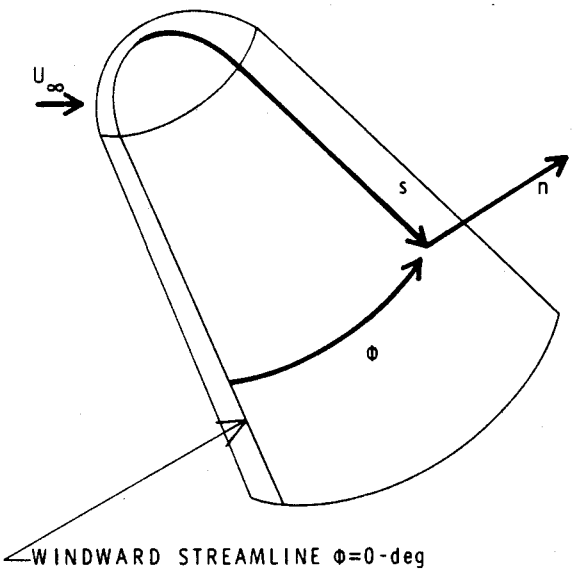

Fig. 1 Coordinate system.

velocity in both cases is 7620 m/s (25,000 ft/s). Although problems with variable wall temperature can be analyzed with this code, in the present study a constant wall temperature of 1000 K is specified. The details of the test case conditions are given in Table 1. The predictions by this method are compared with those from the axisymmetric code (VSL7S) developed by Miner and Lewis.[3,4] Since there are no data available for three-dimensional chemically reacting flow, the results for angle of attack are presented for various ϕ angles around the body.

Analysis

Governing Equations

The viscous shock-layer equations are developed in a body-oriented orthogonal coordinate system (s,n,ϕ), where the s coordinate is tangent to the body in the streamwise direction, n is the coordinate normal to the surface, and the ϕ coordinate is the angle around the body measured from the windward streamline (see Fig. 1). The shock-layer equations are derived from the governing equations for reacting gas mixtures given by Bird et al.[10] or Williams.[11] These equations are first nondimensionalized by variables which are of order one in the region near the body surface and in the inviscid region. The normal velocity v and the normal coordinate n are assumed to be of order ϵ, and up to second-order terms are retained in the conservation equations. The equations are then normalized by the local shock values of the variables to aid in the solution procedure. To avoid division by small numbers, the normal and crossflow velocities v and w are not normalized. Also, the temperature and species concentration are not normalized. The energy and species equations include the rate of production term $\dot{w}_i$ of species i which are functions of both temperature and species concentrations. These terms are rewritten so that the temperature or the species concentration appear as one of the unknowns. The coefficients for the energy and species conservation equation are given in Appendix A. The continuity and momentum equations are unaffected by the inclusion of finite rate chemistry.

Table 1 Test case conditions

Geometry	Rn, m	α, deg	Freestream conditions M_∞	Alt, m	T_∞, K	Re_{Rn}	ϵ	T_w, K
RAMC	0.1524	0, 10	27.18	83,820	182.16	700.5	0.3107	1000
RAMC	0.1524	0, 10	27.18	70,104	219.29	5595.0	0.1052	1000

These equations may be applied throughout a majority of the flowfield; however, there are a few points where the equations become indeterminate. At the blunt stagnation point, the ξ derivatives of the pressure and standoff distance and shock velocity u_{sh} are zero, which creates a singularity in the coefficients of ξ-momentum equations. Another singularity occurs in the continuity equation as ξ approaches zero. The methods used in overcoming these singularities are discussed in detail in Ref. 7. The crossflow velocity is zero in the windward and leeward planes, but the derivative with respect to ζ is nonzero. This is solved by taking the ζ derivative of the crossflow equation, and the resulting equation is solved for a new dependent variable w_ζ, the ζ derivative of w.

Solution Procedure

The equations are written in the standard form

$$A_0\frac{\partial^2 W}{\partial\eta^2}+A_1\frac{\partial W}{\partial\eta}+A_2W+A_3+A_4\frac{\partial W}{\partial\xi}+A_5\frac{\partial W}{\partial\zeta}=0 \qquad (1)$$

The finite-difference method used to solve the ξ-momentum, ζ-momentum, energy, and species equations is the same as that used by Murray and Lewis.[5,6] The continuity and normal momentum equations are solved by a similar method, but they are coupled together. The development of the coupling scheme is given in Ref. 5. The shock standoff distance is evaluated by integrating the continuity equation.

The solution begins on the spherically blunted nose by obtaining an axisymmetric solution in the wind-fixed coordinate system. The axisymmetric solution is rotated into the body-fixed coordinates and is used as the initial profile for the three-dimensional solution. The three-dimensional solution begins in the windward plane and marches around the body obtaining a converged solution at each ζ-step. After completing a sweep in ζ, the procedure then steps downstream in ξ and begins the next ζ-sweep. At each point the equations are solved in the following order: 1) species, 2) ζ-momentum, 3) energy, 4) ξ-momentum, 5) integration of continuity for n_{sh}, and 6) the coupled continuity and normal momentum equations.

The shock-layer equations depend on $\partial n_{sh}/\partial\xi$ and $\partial v/\partial\xi$, which introduce an elliptic effect into the equations. In the present scheme, $\partial n_{sh}/\partial\xi$ is obtained from an inviscid solution and the values of $\partial v/\partial\xi$ are calculated from a backward difference. The solution is globally iterated until convergence.

Boundary Conditions

At the body surface, the no-slip boundary conditions were imposed. The surface conditions are

$$u=v=w=0 \quad \text{and} \quad T=T_w \qquad (2)$$

where T_w is either a constant or a specified temperature variation. For a noncatalytic wall surface (NCW), the species boundary conditions are

$$\partial C_i/\partial\eta=0 \qquad (3)$$

The equilibrium catalytic wall (ECW) conditions are specified by

$$C_i=C_{i_{eq}}(T_w) \qquad (4)$$

In the present work the surface temperatures were sufficiently low that the ECW condition could be approximated by a fully catalytic wall surface (FCW) condition specified by

$$C_O=0,\quad C_{O_2}=0.23456,\quad C_{NO}=0,\quad C_N=0,$$
$$C_{NO^+}=0,\quad \text{and}\quad C_{N_2}=0.76544 \qquad (5)$$

The shock-boundary conditions with slip are the modified Rankine-Hugoniot equations used by Davis.[1] The angle between the freestream velocity vector and a vector tangent to the shock surface and in the plane formed by the normal vector and the freestream velocity vector is denoted by σ. The derivation of σ is given in Refs. 5 and 6. The equations for the conditions behind the shock are given in Appendix B.

Thermodynamic and Transport Properties

The specific heat, C_p, and static enthalpy, h, are required for each of the species considered and for the gas mixture. Also required are the viscosity, μ, and the thermal conductivity, k. Since the multicomponent gas mixture is considered to be a mixture of thermally perfect gases, the thermodynamic and transport properties for each species were calculated using the local temperature. The properties for the gas mixture were then determined in terms of the individual species properties. In this section all expressions are presented in terms of dimensional quantities, and the superscript star will not be used to denote dimensional quantities.

The enthalpy and specific heat data of the species were obtained from the thermodynamic data tabulated by Browne.[12-14] A second-order Lagrangian interpolation was used to obtain the values of $\hat{H}_i$ and $\hat{C}_{pi}$ from the tables. The species enthalpy and specific heat were then obtained from the expressions

$$h_i=T\hat{H}_i+\Delta h_i^F \qquad (6)$$

and

$$C_{p_i}=\hat{C}_{p_i} \qquad (7)$$

where Δh_i^F is the heat of formation of species i.

The viscosity of each of the individual species was calculated from the curve-fit relation

$$\mu_i=\exp(C_i)\,T_k^{(A_i\ln T_k+B_i)} \qquad (8)$$

where A_i, B_i, and C_i are the curve-fit constants for each species from Blottner[15] and T_k is the local temperature in degrees Kelvin.

The thermal conductivity of the individual species was calculated from the Eucken semiempirical formula using the species viscosity and specific heat by the expression

$$k_i=\frac{\mu_i R}{M_i}\left(\frac{C_{p_i}M_i}{R}+\frac{5}{4}\right) \qquad (9)$$

After the viscosity and thermal conductivity of the individual species were calculated, the viscosity and thermal conductivity of the mixture were calculated using Wilke's semiempirical relations:

$$\mu=\sum_{i=1}^{NS}\left(\frac{X_i\mu_i}{\sum_{j=1}^{NS}X_i\phi_{ij}}\right) \qquad (10)$$

$$k=\sum_{i=1}^{NS}\left(\frac{X_ik_i}{\sum_{j=1}^{NS}X_i\phi_{ij}}\right) \qquad (11)$$

where $X_i=C_i\bar{M}/M_i$ and

$$\phi_{ij}=\left[1+\left(\frac{\mu_i}{\mu_j}\right)^{1/2}\left(\frac{M_j}{M_i}\right)^{1/4}\right]^2\left[\sqrt{8}\left(1+\frac{M_i}{M_j}\right)^{1/2}\right]^{-1} \qquad (12)$$

In the present work, the diffusion model is limited to binary diffusion with the binary diffusion coefficients specified by

the Lewis number from

$$Le=\rho C_p D_i/k \tag{13}$$

Chemical Reaction Model

In the present work, it is assumed that the chemical reactions proceed at a finite rate, and the rate of production terms, $\dot{w}_i$, of the individual species are needed. The production terms occur in the energy equation and the species conservation equations. For a multicomponent gas with NS distinct chemical species and NR simultaneous chemical reactions, the chemical reaction equations are written in the general stoichiometric form

$$\sum_{i=1}^{NJ} \alpha_{ri} X_i \underset{k_{br}}{\overset{k_{fr}}{\rightleftharpoons}} \sum_{i=1}^{NJ} \beta_{ri} X_i \tag{14}$$

where $r=1,2,\ldots,NR$ and NJ is equal to the sum of the species and the catalytic third bodies. The quantities X_i represent the chemical species and the catalytic third bodies, and α_{ri} and β_{ri} are the stoichiometric coefficients for reactants and products. The rates at which the forward and backward reactions occur are specified by the forward and backward rate constants which are given by the equations

$$k_{fr}=T_k^{C2_r}\exp(C0_r-C1_r/T_k)$$
$$k_{br}=T_k^{D2_r}\exp(D0_r-D1_r/T_k) \tag{15}$$

where T_k is the temperature in degrees Kelvin. The constants $C0_r$, $C1_r$, $C2_r$, $D0_r$, $D1_r$, and $D2_r$ depend in part on the specific reaction equations chosen. In the present work reaction rate constants were taken from Blottner.[9,15]

As discussed previously, it is desirable to rewrite the expression for the rate of production terms so that the species concentrations appear as one of the unknowns. When rewritten in this way, the rate of production terms are given by the expression

$$\frac{\dot{w}_i}{\rho}=\dot{w}_i^0-\dot{w}_i^1 C_i \tag{16}$$

where

$$\dot{w}_i^0=M_i\sum_{r=1}^{NR}(\Gamma_{ri}^{+}L_{fr}+\Gamma_{ri}^{-}L_{br}) \tag{17}$$

$$\dot{w}_i^1=\sum_{r=1}^{NR}[\Gamma_{ri}^{+}(L_{br}/\gamma_i)+\Gamma_{ri}^{-}(L_{fr}/\gamma_i)] \tag{18}$$

$$\Gamma_{ri}^{+}=(\beta_{ri}-\alpha_{ri}) \quad \text{if} \quad (\beta_{ri}-\alpha_{ri})>0$$
$$=0 \quad \text{if} \quad (\beta_{ri}-\alpha_{ri})\le 0 \tag{19}$$

$$\Gamma_{ri}^{-}=0 \quad \text{if} \quad (\beta_{ri}-\alpha_{ri})\ge 0$$
$$=-(\beta_{ri}-\alpha_{ri}) \quad \text{if} \quad (\beta_{ri}-\alpha_{ri})<0 \tag{20}$$

$$L_{fr}=k_{fr}\bar{\rho}^{\alpha_r}\prod_{j=1}^{NJ}(\gamma_j)^{\alpha_{rj}} \tag{21}$$

$$L_{br}=k_{br}\bar{\rho}^{\beta_r}\prod_{j=1}^{NJ}(\gamma_j)^{\beta_{rj}} \tag{22}$$

$$\alpha_r=\sum_{j=1}^{NJ}\alpha_{rj}-1 \tag{23}$$

$$\beta_r=\sum_{j=1}^{NJ}\beta_{rj}-1 \tag{24}$$

$$\gamma_j=\frac{C_j}{M_j} \qquad j=1,2,\ldots,NS \tag{25}$$

The energy equation requires the rate of production terms rewritten with the temperature appearing as an unknown. That form for the rate of production term was a function of the derivative of $\dot{w}_i/\rho$ with respect to T. With temperature in degrees Kelvin, T_k, the expression for the derivative is

$$\frac{\partial}{\partial T_k}\left(\frac{\dot{w}_i}{\rho}\right)=\frac{M_i}{T_k}\sum_{r=1}^{NR}(\beta_{ri}-\alpha_{ri})[(C2_r+C1_r/T_k-\alpha_r)L_{f_r}$$
$$-(D2_r+D1_r/T_k-\beta_r)L_{br}] \tag{26}$$

With the specification of the chemical kinetics, the system of governing equations for viscous shock-layer flows is complete.

Results and Discussion

Although this code has been developed with options to consider various boundary conditions, only some of them have been exercised at present. At the shock boundary, both shock-slip (SS) and no-shock-slip (NSS) conditions can be imposed. In the present study the effect of shock slip on the electron concentration is looked into in some detail. At the wall, although both equilibrium catalytic wall and noncatalytic wall conditions can be imposed, in the present study only the fully catalytic wall condition is considered. The modifications necessary for including wall slip are being considered for future work.

The results for the test case are presented in two parts. First, the predictions by the present code VSLNEQ are compared with those from the axisymmetric code VSL7S, which helps in verifying the computations by the new code. In nonequilibrium flow, the electron concentration is one of the important results to be obtained; hence, the electron concentration profile at $s/Rn=8.8$ is compared with the experimental results. In the second part the three-dimensional results are presented.

Figures 2-6 show the computational results for zero angle of attack at 83.82 km (275 kft) altitude from the axisymmetric code VSL7S, and the new three-dimensional code VSLNEQ. The surface-measurable quantities are presented for the no-shock-slip condition, whereas the electron concentration profiles are presented for both shock-slip and no-shock-slip cases. Figure 2 shows the shock standoff distance predicted by VSL7S and VSLNEQ. These results are output from the second global iteration. On the sphere, the predictions by both codes are in excellent agreement, whereas, on the cone, the shock standoff distance predicted by VSLNEQ is higher. The

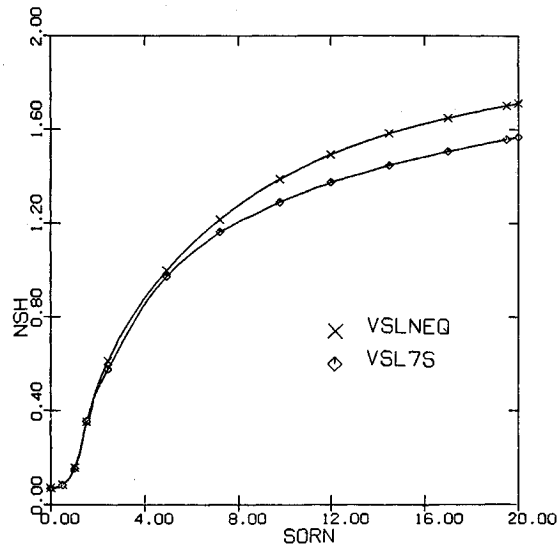

Fig. 2 Shock standoff distance for $\alpha=0$ deg.

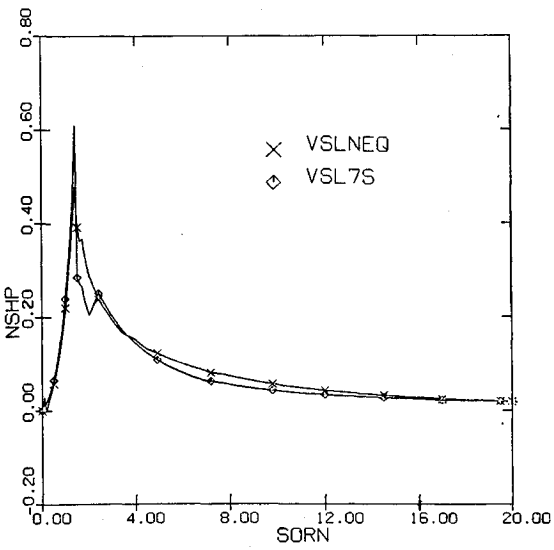

Fig. 3 Shock slope distribution for $\alpha = 0$ deg.

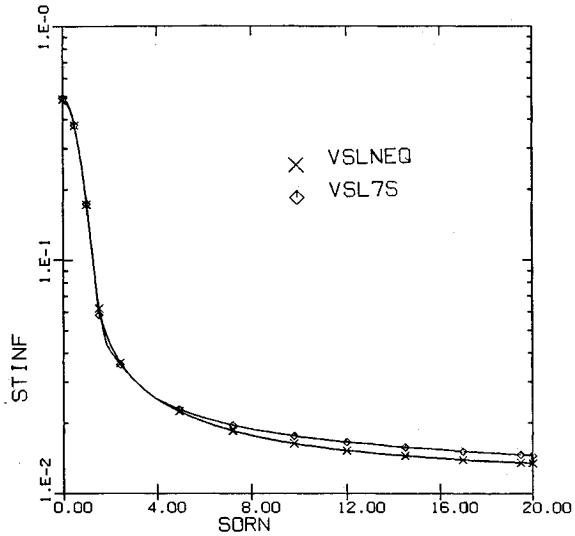

Fig. 4 Surface heat-transfer distribution for $\alpha = 0$ deg.

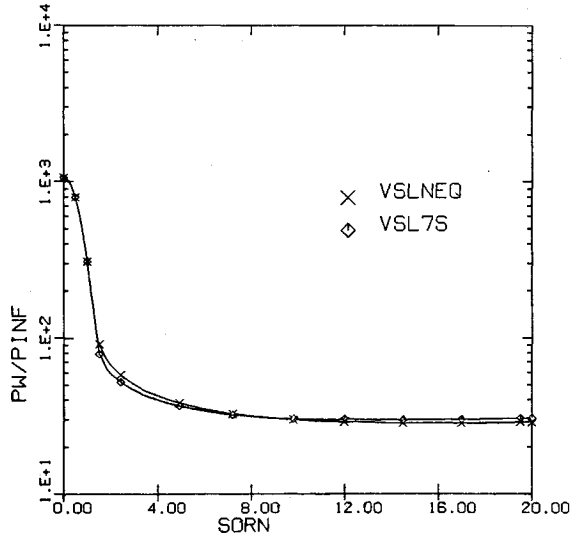

Fig. 5 Surface pressure distribution for $\alpha = 0$ deg.

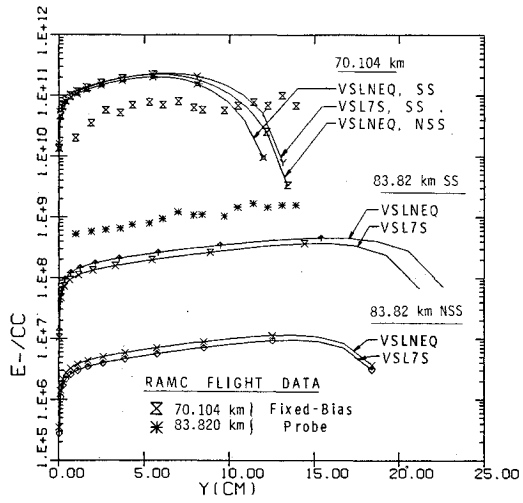

Fig. 6 Electron concentration at $s/Rn = 8.8$ for $\alpha = 0$ deg.

maximum difference of 20% is observed at the end of the body. In Fig. 3 the shock slope computed by both codes is shown, and the predictions by both codes are in good agreement.

Figures 4 and 5 show the surface-measurable quantities for zero angle of attack. Once again these results are output from the second global iteration. Figure 4 shows the surface heat-transfer distribution predicted by both codes, and the results are in excellent agreement. The surface pressure predictions by both codes are in good agreement (Fig. 5).

Figure 6 shows the electron concentration profile at $s/Rn = 8.8$ for various boundary conditions and at the two altitudes under consideration. Computations for both shock slip and no shock slip are made, and the results are presented. All the computations are made with no wall slip and for a fully catalytic wall. The results from the two codes are within 15% of each other for all the cases considered. The measurements by a fixed bias probe are presented for comparison. From the figure the effects of shock slip on the production of electrons can be obtained. At 83.82 km (275 kft) the low-density effects are more predominant, and the computation with no shock slip gives the electron concentration about two orders lower than the experiment. With shock slip the results are closer to the experimental results. Still both codes underpredict the electron concentration at 83.82 km (275 kft) by about a factor of four. These computations are made with no wall slip, and at this altitude the low-density effects are important, thus making it necessary to include the wall-slip effects into the computations. It is felt that the wall-slip effects will change the temperature profile considerably and this will, in turn, change the electron concentration. In future studies it is planned to modify the code for wall slip and the effect of wall slip will be studied. At 70.104 km (230 kft) the shock-slip effects are negligible. Surprisingly both the codes overpredict the electron concentration at 70.104 km (230 kft).

From the above results it is seen that the results from the new code agree well with those from the axisymmetric code. Once the accuracy has been established, the three-dimensional results are presented. To the best of these authors' knowledge, there are no three-dimensional results for nonequilibrium flow available for similar conditions; hence, these results are presented for various ϕ angles around the body. Figure 7 shows the shock standoff distance for various ϕ planes. For a comparison the inviscid input is also presented. Figure 8 shows the surface heat-transfer distribution for three different ϕ planes, and, as expected, the maximum heat transfer is observed in the windward plane. Figure 9 shows the surface pressure results for $\alpha = 10$ deg. These results are the output from the second global iteration. Figure 10 shows the circumferential pressure distribution at the end of the body.

The computing times required for analyzing the nonequilibrium flowfield under these conditions are com-

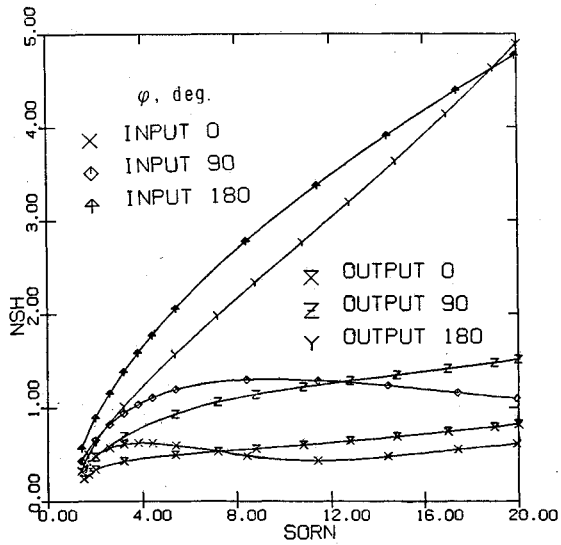

Fig. 7 Shock standoff distance for $\alpha = 10$ deg.

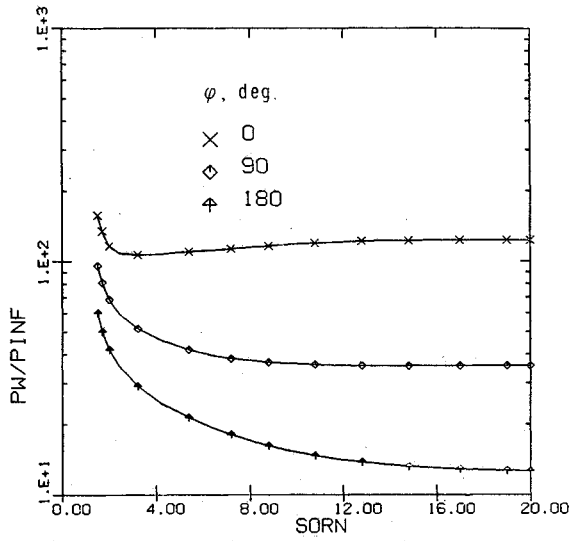

Fig. 9 Surface pressure distribution for $\alpha = 10$ deg.

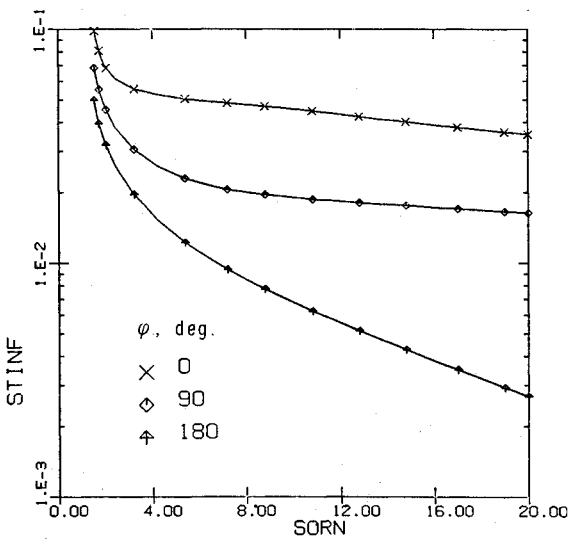

Fig. 8 Surface heat-transfer distribution for $\alpha = 10$ deg.

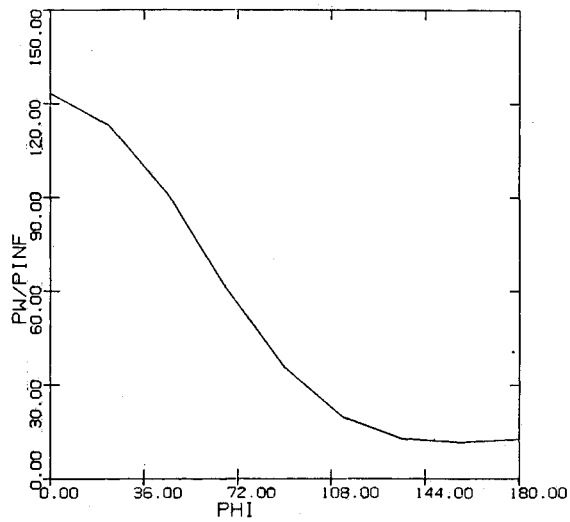

Fig. 10 Circumferential pressure distribution at $s/Rn = 20$, $\alpha = 10$ deg.

pared with those required for perfect gas in Table 2. The nonequilibrium calculations require about an order of magnitude more computing time than the perfect gas. In general, the computing time is more for shock-slip cases. At the lower altitude the flow is closer to equilibrium; hence, the nonequilibrium code requires more time for the solution. It should be noted, however, that all the present three-dimensional, finite-rate, chemically reacting, laminar, hypersonic, viscous flowfield solutions have been obtained in reasonable computing times on a general-purpose computer (IBM 370/3032). Predictions using any time-dependent Navier-Stokes code would require at least 1 h of CDC 7600 time and would be prohibitive on a general-purpose computer.

Concluding Remarks

From these results it is seen that a viscous shock-layer method for solving the three-dimensional nonequilibrium

Table 2 Computing times[a] for test case

α, deg	Alt, m	Method	Flow type	ξ	ξ-Steps	Grid size[b] η-Points	ζ-Planes	Time (min:sec)	Time[c] ratio
0	83,820	VSLNEQ	NSS	0.0-20.0	57	51	1	4:43	1.00
0	83,820	VSLNEQ	SS	0.0-20.0	57	51	1	5:42	1.21
0	83,820	VSL7S	NSS	0.0-20.0	57	51	1	5:19	1.13
0	83,820	VSL7S	SS	0.0-20.0	57	51	1	6:04	1.28
0	70,104	VSLNEQ	NSS	0.0-20.0	57	51	1	5:15	1.11
0	70,104	VSL7S	SS	0.0-20.0	57	51	1	6:07	1.30
10	83,820	VSLNEQ	NSS	0.0-20.0	41	51	9	21:16	9.00
10	70,104	VSLNEQ	NSS	0.0-20.0	43	51	9	26:00	11.00
10	83,820	VSL3D	PG	0.0-20.0	43	51	9	2:00	1.00

[a]CPU time on IBM 370/3032, H=OPT2 compiler. [b]Core requirements: VSL7S, 255 kbytes. VSLNEQ, 265 kbytes. [c]Reference: 83.82 km NSS VSLEQ for $\alpha = 0$ deg; 83.82 km perfect gas for $\alpha = 10$ deg.

flow over axisymmetric, blunted sphere-cones within reasonable computing time is developed. The surface-measurable quantities for zero lift are in good agreement with those from an earlier axisymmetric code. The production of electrons predicted by the three-dimensional code, VSLNEQ, is in good agreement with the predictions by the axisymmetric code VSL7S. In conclusion, a method for analyzing the three-dimensional, nonequilibrium flow is demonstrated.

Appendix A

The coefficients for energy and species conservation equations are as follows.

Energy:

$$A_0 = -\frac{\epsilon^2 \bar{k} k_{sh}}{n_{sh}^2} \tag{A1}$$

$$A_1 = \frac{\tilde{\rho}\rho_{sh} v C_p}{n_{sh}} - \frac{\tilde{\rho}\rho_{sh}\tilde{u}u_{sh}C_p\eta}{h_1 n_{sh}}\left(\frac{\partial n_{sh}}{\partial \xi}\right) - \tilde{\rho}\rho_{sh} w C_p \eta\left(\frac{\partial n_{sh}}{\partial \zeta}\right) - \frac{\epsilon^2 k_{sh}}{n_{sh}^2}\left(\frac{\partial \bar{k}}{\partial \eta}\right) - \frac{\epsilon^2 \bar{k} k_{sh}}{h_3 n_{sh}^2}\frac{\partial h_3}{\partial \eta} - \frac{\epsilon^2 \bar{k} k_{sh}}{h_1 n_{sh}^2}\left(\frac{\partial h_1}{\partial \eta}\right) + \frac{\epsilon^2 (\Sigma J_i C_{pi})}{n_{sh}} \tag{A2}$$

where

$$J_i = -\frac{\mu}{Pr} Le_i \frac{\partial C_i}{\partial y}$$

$$A_2 = \dot{w}_2 \tag{A3}$$

$$A_3 = -\frac{p_{sh}\tilde{u}u_{sh}}{h_1}\frac{\partial \tilde{p}}{\partial \xi} - \tilde{u}u_{sh}\tilde{p}\left(\frac{\partial p_{sh}}{\partial \xi}\right) + p_{sh}\tilde{u}u_{sh}\eta\left(\frac{\partial n_{sh}}{\partial \xi}\right)\left(\frac{\partial \tilde{p}}{\partial \eta}\right) - \frac{p_{sh}}{n_{sh}} v\left(\frac{\partial \tilde{p}}{\partial \eta}\right) - \frac{w}{h_3}\frac{\partial(\tilde{p}p_{sh})}{\partial \zeta} + \frac{p_{sh} w \eta}{h_3 n_{sh}}\left(\frac{\partial n_{sh}}{\partial \zeta}\right)\frac{\partial \tilde{p}}{\partial \eta} - \epsilon^2 \tilde{\mu}\mu_{sh}\left[\frac{u_{sh}}{n_{sh}}\frac{\partial \tilde{u}}{\partial \eta} - \frac{\tilde{u}u_{sh}}{h_1 n_{sh}}\left(\frac{\partial h_1}{\partial \eta}\right)\right]^2 - \epsilon^2 \tilde{\mu}\mu_{sh}\left[\frac{\left(\frac{\partial w}{\partial \eta}\right)}{n_{sh}} - \frac{w\left(\frac{\partial h_3}{\partial \eta}\right)}{h_3 n_{sh}}\right]^2 + \dot{w}_1 \tag{A4}$$

$$A_4 = \frac{\tilde{\rho}\rho_{sh}\tilde{u}u_{sh}C_p}{h_1} \tag{A5}$$

$$A_5 = \frac{\tilde{\rho}\rho_{sh}\tilde{w}C_p}{h_3} \tag{A6}$$

Species:

$$A_0 = \frac{\epsilon^2}{n_{sh}^2}\frac{\mu_{sh}\tilde{\mu}Le}{Pr} \tag{A7}$$

$$A_1 = \frac{\epsilon^2}{n_{sh}^2}\frac{\partial}{\partial \eta}\left(\frac{\mu_{sh}\tilde{\mu}Le}{Pr}\right) + \frac{\epsilon^2}{n_{sh}}\frac{1}{h_3}\frac{\tilde{\mu}\mu_{sh}Le}{Pr}\frac{\partial h_3}{\partial \eta} + \frac{\epsilon^2}{n_{sh}^2}\frac{1}{h_1}\frac{\tilde{\mu}\mu_{sh}Le}{Pr}\frac{\partial h_1}{\partial \eta} + \frac{\tilde{\rho}\rho_{sh} w}{h_3}\frac{\eta}{n_{sh}}\frac{\partial n_{sh}}{\partial \zeta} + \frac{\tilde{\rho}\rho_{sh}\tilde{u}u_{sh}}{h_1}\frac{\eta}{n_{sh}}\frac{\partial n_{sh}}{\partial \xi} - \frac{\tilde{\rho}\rho_{sh} v}{n_{sh}} \tag{A8}$$

$$A_2 = -\rho_{sh}\tilde{\rho}\dot{w}_i^1 \tag{A9}$$

$$A_3 = \rho_{sh}\tilde{\rho}\dot{w}_i^0 \tag{A10}$$

$$A_4 = -\frac{\tilde{\rho}\rho_{sh}\tilde{u}u_{sh}}{h_1} \tag{A11}$$

$$A_5 = -\frac{\tilde{\rho}\rho_{sh} w}{h_3} \tag{A12}$$

Appendix B

Shock boundary conditions:

$$\tilde{u}_{sh} = \frac{\cos\sigma}{1 + \frac{\epsilon^2}{n_{sh}}\frac{\mu_{sh}}{\sin\sigma}\left(\frac{\partial \tilde{u}}{\partial \eta}\right)} \tag{B1}$$

$$T_{sh} = \frac{0.5(\tilde{u}_{sh} - \cos\sigma)^2 + 0.5(\sin^2\sigma - \tilde{v}_{sh}^2) + \sum_{i=1}^{NS} C_{i_\infty} h_{i_\infty}}{\sum_{i=1}^{NS} C_{i_\infty}\left(\frac{h_{ish}}{T_{sh}}\right) + \frac{\epsilon^2 k_{sh}}{n_{sh}\sin\sigma}\left(\frac{\partial \bar{T}}{\partial \eta}\right)} \tag{B2}$$

$$p_{sh} = \frac{p_\infty}{\rho_\infty U_\infty^2} + \sin\sigma(\tilde{v}_{sh} + \sin\sigma) \tag{B3}$$

$$\rho_{sh} = \frac{p_{sh}}{T_{sh}\left(\frac{R}{C_{pref}}\right)} \tag{B4}$$

$$\tilde{v}_{sh} = -\frac{\sin\sigma}{\rho_{sh}} \tag{B5}$$

$$C_{i_{sh}} = C_{i_\infty} - \epsilon^2\left(\frac{\mu Le_i}{Pr}\right)_{sh}\frac{1}{n_{sh}}\frac{\partial C_i}{\partial \eta}\frac{1}{\sin\sigma} \tag{B6}$$

References

[1] Davis, R.T., "Numerical Solution of the Hypersonic Viscous Shock-Layer Equations," *AIAA Journal,* Vol. 8, May 1970, pp. 843-851.

[2] Srivastava, B.N., Werle, M.J., and Davis, R.T., "Stagnation Region Solutions of the Full Viscous Shock-Layer Equations," *AIAA Journal,* Vol. 14, Feb. 1976, pp. 274-276.

[3] Miner, E.W. and Lewis, C.H., "Hypersonic Ionizing Air Viscous Shock-Layer Flows over Nonanalytic Blunt Bodies," NASA CR-2550, May 1975; also *AIAA Journal,* Vol. 14, Jan. 1976, pp. 64-69.

[4] Miner, E.W. and Lewis, C.H., "Computer User's Guide for a Chemically Reacting Viscous Shock-Layer Program," NASA CR-2551, May 1975.

[5] Murray, A.L. and Lewis, C.H., "Three Dimensional Fully Viscous Shock-Layer Flows Over Sphere-Cones at High Altitudes and High Angles of Attack," VPI-AERO-078, March 1975.

[6] Murray, A.L. and Lewis, C.H., "Hypersonic Three-Dimensional Viscous Shock-Layer Flow over Blunt Bodies," *AIAA Journal,* Vol. 16, Dec. 1978, pp. 1279-1286.

[7] Szema, K.Y. and Lewis, C.H., "Three-Dimensional Hypersonic Laminar, Transitional and/or Turbulent Shock-Layer Flows," *Journal of Spacecraft and Rockets,* Vol. 19, Jan. 1982, pp. 88-91.

[8] Thareja, R.R., Szema, K.Y., and Lewis, C.H., "Effects of Chemical Equilibrium on Three-Dimensional Viscous Shock-Layer Analysis of Hypersonic Laminar or Turbulent Flows," AIAA Paper 82-0305, Jan. 1982.

[9] Blottner, F.G., "Nonequilibrium Laminar Boundary Layer Flow of Ionized Air," Rept. R64SD56, Space Sciences Laboratory, General Electric Co., Philadelphia, Pa., Nov. 1964.
[10] Bird, R.B., Stewart, W.E., and Lightfoot, E.N., *Transport Phenomena,* John Wiley and Sons, Inc., 1960.
[11] Williams, F., *Combustion Theory,* Addison-Wesley Book Co., Inc., 1965.
[12] Browne, W.G., "Thermodynamic Properties of Some Atoms and Atomic Ions," MSD Engineering Physics TM2, General Electric Co., Philadelphia, Pa.
[13] Browne, W.G., "Thermodynamic Properties of Some Diatomic and Linear Polyatomic Molecules," MSD Engineering Physics TM3, General Electric Co., Philadelphia, Pa.
[14] Browne, W.G., "Thermodynamic Properties of Some Diatoms and Diatomic Ions at High Temperature," MSD Advanced Aerospace Physics TM8, General Electric Co., Philadelphia, Pa., May 1962.
[15] Blottner, F.G., Johnson, M., and Ellis, M., "Chemically Reacting Viscous Flow Program for Multi-Component Gas Mixtures," Rept. SC-RR-70-754, Sandia Laboratories, Albuquerque, N. Mex., Dec. 1971.